IET Microwaves, Antennas & Propagation

Research Article

Design and measurements of a tri-band one-dimensional electromagnetic bandgap resonator antenna

ISSN 1751-8725
Received on 29th April 2015
Revised on 1st August 2015
Accepted on 27th August 2015
doi: 10.1049/iet-map.2015.0301
www.ietdl.org

Basit A. Zeb ✉, *Karu P. Esselle*

Centre for Electromagnetic and Antenna Engineering, Department of Engineering, Macquarie University, Sydney, New South Wales 2109, Australia
✉ *E-mail: basit.zeb@mq.edu.au*

Abstract: The authors utilise a one-dimensional (1D) stack of three identical unprinted dielectric slabs as a superstructure to design a novel yet simple tri-band electromagnetic bandgap resonator antenna (ERA). The design, inspired from classical single-band 1D ERAs, is conceived by creating two resonant defects in the superstructure configuration to make it suitable for tri-band and high gain operation. A prototype, fabricated using FR4 material, is tested with a waveguide-fed slot antenna at 10.3, 11.9 and 13.7 GHz with a frequency ratio of 1.33:1.16:1. The slot feeds the cavity simultaneously in the three frequency bands and provides good impedance matching in each frequency band. Peak measured gains of 14.3, 13.4 and 16.1 dBi and radiation efficiencies of 83, 85 and 85% are achieved in the lower, middle and higher frequency bands, respectively.

1 Introduction

Electromagnetic bandgap (EBG) resonator antennas (ERA), also known as Fabry–Perot cavity antennas or two-dimensional (2D) leaky-wave antennas [1–4], are planar high-gain antennas that employ a Fabry–Perot cavity which is formed between a partially but sufficiently reflecting superstructure and a conducting ground plane. Typically, a small less-directive antenna close to the ground plane feeds the cavity from the centre. The electromagnetic waves radiated by the feed antenna undergo multiple partial reflections and transmissions. The partially transmitted waves through the superstructure form a highly directive boresight beam [5]. This phenomenon results in cavity resonance leading to a narrowband ERA due to high Q factor of the cavity.

Since the pioneering work of Von Trentini in 1956 [5], several design techniques to improve the performance of ERAs in multiple or wide frequency bands have been investigated [6–19]. To achieve multi-frequency or wideband operation in such ERAs, besides the requirement of having a suitable feed, the superstructure employs at least two resonant defects or inclusions. These resonant defects are realised using defect dielectric slabs/rods or printed elements depending on whether the superstructure is a 1D stack of unprinted dielectric slabs [4], a 2D printed frequency selective surface (FSS) [6], a 2D array of dielectric rods [7] or a 3D volumetric structure such as a EBG woodpile [20]. We recently demonstrated how a simple 1D EBG superstructure made out of two identical dielectric slabs and hosting one inter-slab resonant cavity defect [21, 22] is suitable for dual-band operation when its reflection phase is engineered properly. This dual-band design can be conveniently modified to obtain tri-band operation by incorporating an additional resonant cavity defect as described in our preliminary theoretical work [23].

In this paper, we present the detailed design and measurements of a novel and functional tri-band ERA for the first time. The key features are a simple 1D superstructure made out of three identical dielectric slabs and the use of only two resonant defects to achieve cavity resonance in three frequency bands. We first analyse the reflection of the unit-cell superstructure model (SM) and transmission through the defect-cavity model (DCM) [24]. We then evaluate the performance of the entire antenna using full-wave simulations through the commercial numerical electromagnetic solver CST Microwave Studio (CST MWS) [25]. Initially, three simple microstrip patch antennas, one for each band, are used to predict the directivity enhancement in each frequency band. Later on, a single waveguide-fed slot is designed to cover all three frequency bands simultaneously. We also present the results of tuning the frequency ratio using full-wave parametric simulations. Finally, a prototype is fabricated and tested.

2 Design and configuration

The proposed configuration of the tri-band ERA is shown in Fig. 1. Its superstructure consists of three unprinted dielectric slabs with equal thickness (t) and permittivity (ϵ_r) and forms a half-wavelength thick (h) resonant cavity with a perfect electric conductor (PEC) ground plane. Any type of small feed antenna can be used; we found that a slot antenna with wideband performance can cover all three frequency bands.

The design is inspired from a classical single-band ERA in which three quarter-wavelength thick dielectric slabs are spaced quarter-wavelength apart ($h_1 = h_2 = 0.25\lambda_0$), where λ_0 is the free-space wavelength at design frequency. Its classical superstructure, with a reflection coefficient $R = |\Gamma_{sup}| \cdot e^{j\psi}$, has close-to-ideal reflection phase, that is, the phase condition

$$\psi - \pi - 4\pi h/\lambda_0 = 2N\pi \tag{1}$$

is satisfied only in one narrow frequency band, where N is integer. Such superstructures can be modified to achieve correct phase for tri-band operation. We achieve this by creating two resonant inter-slab cavities with heights h_1 and h_2 such that the phase condition is satisfied in three distinct frequency bands. In other words, the proposed ERA exhibits three defect modes with near-perfect transmission. Hence, one can analyse the reflection and transmission characteristics of the unit-cell superstructure to understand the working principle of the antenna.

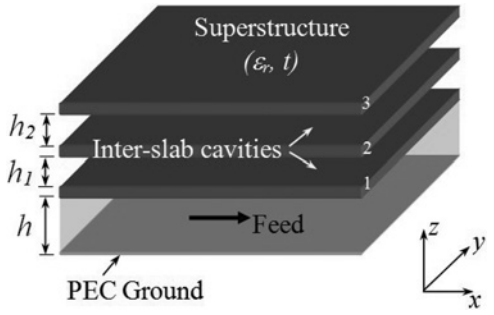

Fig. 1 *Configuration of the tri-band 1D EBG resonator antenna. Two inter-slab air cavities are formed within the three dielectric slabs of the superstructure*

3 Superstructure for tri-band operation: unit-cell analysis

Let us consider a superstructure made out of three FR4 slabs (ε_r = 4.4, tanδ = 0.02). The design frequency is 12 GHz for the convenience of prototyping. Fig. 2 shows the two unit-cell models: SM and DCM that are used to compute the reflection and transmission characteristics of the ERA using the time-domain solver of CST MWS. In the unit-cell simulation setup, perfect E and perfect H boundary conditions were applied to lateral side walls (x and y directions), and normally incident plane wave excitations were defined at the two ports. The phase and magnitude of the superstructure's reflection coefficient (Γ_{sup}) is calculated at the bottom of the first slab in SM, as shown in Fig. 2*a*, using the port de-embedding feature within the software. In DCM, the transmission ($|\tau_{DCM}|$) is defined from port 1 to port 2, that is, from the bottom image slab (closer to port 1) to the top main slab (closer to port 2) when port de-embedding feature is used.

3.1 SM and reflection analysis

To obtain the desired reflection characteristics for tri-band operation, we carefully adjusted the heights of the inter-slab cavities (h_1 and h_2) to create two defect resonances and computed the phase and magnitude of the superstructure's reflection coefficient (Γ_{sup}) using SM. The reflection phase results are shown in Fig. 3. Overall, the reflection phase decreases with frequency except at two defect-resonance frequencies, f_{res1} and f_{res2}, where it is locally inverted to have a positive phase gradient, as shown in Fig. 3, due to the resonances of the inter-slab cavities. This phase inversion was observed to be more abrupt for EBG structures made out of low-loss dielectric materials. For the given main-cavity height h, an ideal superstructure phase exists that makes the main cavity resonate at any given frequency, that is, phase increases linearly with frequency. This ideal phase, obtained using the phase condition in (1), and the reflection phase of the classical superstructure are also shown in Fig. 3.

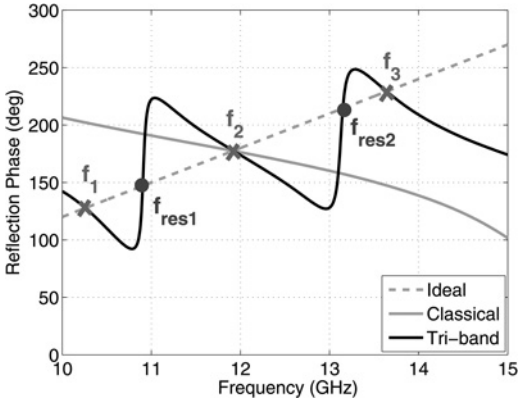

Fig. 3 *Reflection phase characteristics of the superstructure. Slab material is FR4, thickness t = 3.175 mm, h = 12.5 mm, $h_1 = h_2$ = 12.1 mm*

Note that the ideal and superstructure reflection phase curves intersect each other at five distinct frequency points, which are labelled as f_1, f_2, f_3, f_{res1} and f_{res2}. Although, the reflection phase is correct for main-cavity resonance at f_{res1} and f_{res2}, the reflection-coefficient magnitude of the superstructure ($|\Gamma_{sup}|$), shown in Fig. 4, is not sufficiently large (≥0.6) at f_{res1} and f_{res2}. In fact, the superstructure appears transparent to the waves radiated by the feed at f_{res1} and f_{res2} because $|\Gamma_{sup}|$ is close to zero (~0.05) and hence, the main cavity does not resonate. In other words, the necessary conditions of directivity enhancement are not satisfied at these two frequencies. At the other three frequencies (f_1, f_2 and f_3), sufficiently large reflection-coefficient magnitudes ($|\Gamma_{sup}| \sim 0.6$) will result in directivity enhancement. Hence, the SM gives useful insight into the design of superstructure for tri-band operation.

Using parametric simulations, we found that the optimal values of h_1 and h_2 to satisfy cavity resonance condition in three frequency bands are in the range of 0.47–0.5λ_0. Increasing these values beyond 0.5λ_0 result in a decrease in the superstructure reflectivity and the cavity-resonance frequency ratio (f_3:f_2:f_1) as well as an increase in the total height of the antenna.

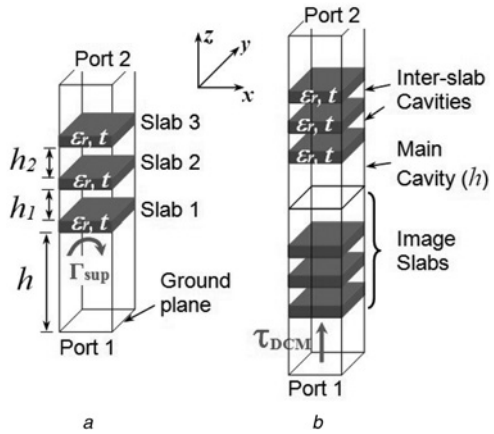

Fig. 2 *Unit-cell models. DCM is obtained by removing the ground plane and adding image dielectric slabs. Port 1 is excited by a normally incident plane wave*

a Superstructure model
b Defect-cavity model

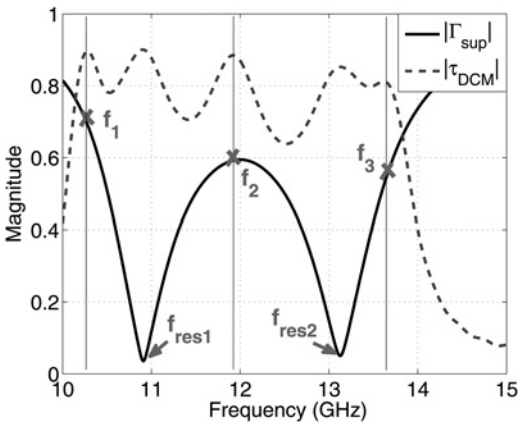

Fig. 4 *Transmission through the DCM and reflection of the SM. Reflection magnitudes ($|\Gamma_{sup}|$) of the superstructure at three cavity resonance frequencies, f_1, f_2 and f_3, are 0.7, 0.6 and 0.58, respectively*

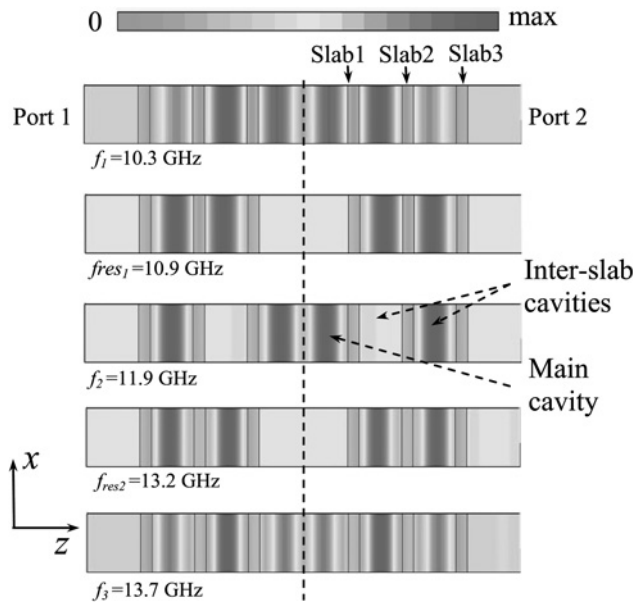

Fig. 5 *Tangential electric field component (E_x) inside the DCM. Note the presence of travelling waves in the main cavity at f_{res1} and f_{res2}, and standing waves at f_1, f_2 and f_3. Dotted line represents the symmetry plane*

3.2 DCM and transmission analysis

By computing the transmission through DCM ($|\tau_{DCM}|$), shown in Fig. 4, one can observe transmissions peaks (with a magnitude of ~0.9) at three potential operating frequencies f_1, f_2 and f_3. Since $|\tau_{DCM}|$ curve has transmission peaks at f_{res1} and f_{res2} in addition to f_1, f_2 and f_3, DCM can be used to tune the three antenna operating frequencies. Due to losses in both the image and the main dielectric slabs, it is noted that the transmission peaks at f_{res2} and f_3 tend to merge. Further analysis using electric field distributions inside DCM and observation of the reflection magnitudes at these frequencies helped us to select f_3 as the third operating frequency. It was also observed that perfect transmission (i.e., $|\tau_{DCM}| = 1$) occurred at f_{res2} and f_3 when the slabs are assumed to be lossless making the two transmission peaks fairly distinguishable.

The magnitude of the tangential electric field component through DCM, plotted in Fig. 5, reveals the existence of dominating standing waves in the main cavity due to cavity resonance at these three frequencies. On the contrary, the main cavity has travelling waves instead of standing waves at f_{res1} and f_{res2} which means that the whole superstructure is transparent and hence, no directivity enhancement is possible at these frequencies. Since the tangential electric field component vanishes at the symmetry plane only at f_1, f_2 and f_3, an antenna can be formed by placing a conducting ground plane at the symmetry plane and by removing the image slabs.

Thus, SM and DCM are computationally efficient tools to predict the directivity enhancement in three frequency bands and to tune the superstructure to three frequencies. They also give useful insight into the working principle of the ERA and their simultaneous use adds confidence to the design process. The reflection and transmission analyses are then followed by full-wave simulations of a finite-size ERA with actual feed.

4 Full-wave simulations

As a practical example, a finite-size ERA is formed by truncating the superstructure area and placing a suitable feed source above a PEC ground plane. Here, three 3.17 mm-thick unprinted dielectric slabs of FR4 material are considered. The parameters h, h_1 and h_2 are adjusted to 12.1, 12.7 and 12.7 mm to tune the operating frequencies to 10.3, 11.9 and 13.7 GHz, respectively. This

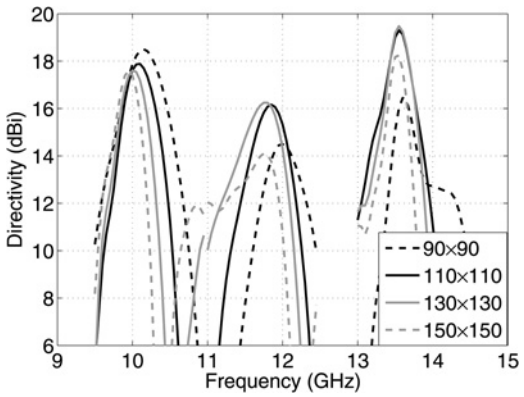

Fig. 6 *Computed boresight directivity of ERA for different superstructure areas. Three probe-fed microstrip patches, one for each band and printed on 0.787 mm-thick Rogers Duroid 5880 material, are used. Dimensions of the three patches are 8.8 × 12.5, 7.5 × 12 and 6.5 × 9.8 mm^2, for the lower, middle and higher frequency band, respectively*

corresponds to a frequency ratio of 1.33:1.16:1. We first considered probe-fed microstrip patch antennas, one for each band, to feed the cavity separately and then a waveguide-fed slot antenna to cover all three bands simultaneously.

4.1 Optimisation of superstructure area and feed design

Our design objective is to optimise the superstructure area for best overall directivity in all three frequency bands. We investigated the effect of changing the superstructure area on peak directivity numerically using CST MWS. The results are shown in Fig. 6. As can be seen, equally good performances are achieved when the superstructure areas are 110×110 and 130×130 mm^2. The peak directivity is 17.8 dBi at 10.3 GHz, 16.3 dBi at 11.85 GHz and 18.1 dBi at 13.65 GHz. For design compactness, we chose the superstructure area to be 110×110 mm^2.

We then considered a waveguide-fed slot antenna to feed the cavity. Such a feed is desirable for practical applications where all three bands can be used simultaneously using one input radio-frequency connector. We anticipated lower peak directivity of the ERA using the slot feed as compared with the patch feed because the slot radiation is not optimal in each frequency band even though it is designed to provide good impedance matching ($|S_{11}| < -10$ dB) in all three frequency bands. The computed input reflection coefficient and the peak directivity of the ERA with the slot feed are shown in Fig. 7. The peak directivity is 15.1 dBi at 10.25 GHz, 13.5 dBi at 11.85 GHz and 15.7 dBi at 13.65 GHz which is lower than the values obtained using the patch feed.

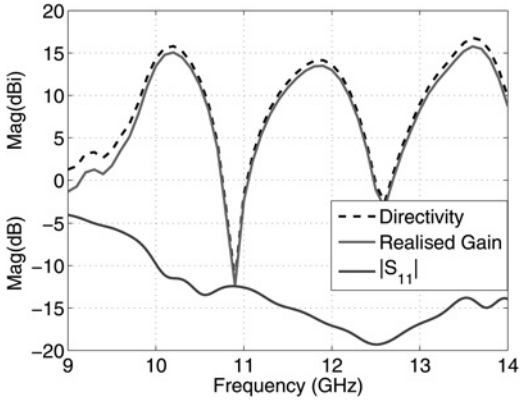

Fig. 7 *Computed directivity, gain and $|S_{11}|$ of the ERA using the slot feed. Slot dimensions are 14 × 9.2 mm^2*

IET Microw. Antennas Propag., 2016, Vol. 10, Iss. 2, pp. 168–172

Table 1 Results of parametric study for tuning the frequency ratio using full-wave antenna simulations

Parameters (normalised to λ_1)			f_3:f_2:f_1 ratio
t	h_1	h_2	
0.103 (2.98 mm at f_1)	0.39	0.39	1.34:1.16:1
	0.39	0.455	1.37:1.14:1
	0.44	0.39	1.34:1.20:1
	0.44	0.405	1.33:1.19:1
0.109 (3.175 mm at f_1)	0.38	0.445	1.36:1.13:1
	0.395	0.38	1.35:1.17:1
	0.412	0.395	1.34:1.18:1
	0.435	0.435	1.33:1.16:1
0.123 (3.58 mm at f_1)	0.35	0.412	1.35:1.11:1
	0.371	0.371	1.34:1.16:1
	0.371	0.432	1.38:1.15:1
	0.392	0.432	1.30:1.14:1
0.139 (4.05 mm at f_1)	0.315	0.41	1.36:1.10:1
	0.315	0.315	1.33:1.16:1
	0.384	0.34	1.37:1.19:1
	0.41	0.384	1.35:1.18:1

Superstructure area is $3.78\lambda_1 \times 3.78\lambda_1$ (110×110 mm^2 for $f_1 = 10.3$ GHz). $h = 0.415\lambda_1$.

4.2 Tuning the frequency ratio (f_3:f_2:f_1)

It is possible to tune the antenna frequency ratio by adjusting the parameters t, h_1 and h_2 for a given superstructure area or by changing the superstructure area while keeping t, h_1 and h_2 fixed. Here, we consider the former case and performed a parametric study of the antenna for different combinations of t, h_1 and h_2 for a fixed superstructure area. The parameters ϵ_r and h were set to 4.4 and 12 mm, respectively. We recorded the peak values of directivity (≥12 dBi) in each frequency band and then calculated the frequency ratio. The key results are shown in Table 1. For the convenience of scaling these results to other frequency bands, the antenna dimensions are normalised to λ_1. We found that when $h_1 = h_2$ for all the values of t considered, a nearly fixed frequency ratio of 1.34:1.16:1 is achieved, while for other values of h_1 and h_2 the frequency ratios f_2/f_1 and f_3/f_1 are in the range of 1.10–1.20 and 1.30–1.38, respectively. We also found that increasing the slab thickness beyond $0.139\lambda_1$ not only leads to a degradation in peak directivity in the middle and higher frequency bands but also results in smaller frequency ratios.

We wish to point out here that the tri-band design is conceived from the dual-band ERA which employs only one inter-slab cavity formed between two identical dielectric slabs [22]. Conceptually, it is possible to extend the tri-band design to achieve quad-band operation by simply incorporating an additional resonant cavity in the superstructure. However, additional cavities can affect the peak directivity and sidelobe levels of the resulting antenna besides increasing the total height of the antenna. Furthermore, a separate feed source, one for each band, or a very wideband antenna may be required to feed the cavity.

5 Prototype fabrication and measurements

Fig. 8 shows the photographs of the prototype ERA. A slot aperture, made in a 1 mm-thick aluminium ground plane, is fed by a commercial 50 Ω WR75 waveguide-to-coax adaptor. Nylon spacers were used to hold the FR4 slabs above the ground plane. The parameters h, h_1 and h_2 were adjusted to 12.1, 12.7 and 12.7 mm (they correspond to $0.415\lambda_1$, $0.435\lambda_1$ and $0.435\lambda_1$ in Table 1), respectively. The input reflection coefficient and gain of the ERA were measured using a PNA-X N5242A vector network analyser and a NSI-700S-50 spherical near-field antenna range, respectively, and the results are shown in Fig. 9.

The gain of the prototype antenna was measured by the gain comparison method using a standard gain horn as the reference antenna. Peak measured directivities are 15.1, 14.1 and 16.8 dBi at $f_1 = 10.2$ GHz, $f_2 = 11.9$ GHz and $f_3 = 13.7$ GHz, respectively. The measured gains are 14.3, 13.4 and 16.1 dBi while the corresponding radiation efficiencies are 83, 85 and 85% in the lower, middle and higher frequency bands, respectively. The radiation efficiency can be increased by reducing the dielectric losses, for example, by fabricating a superstructure with low-loss materials such as TMM4 ($\tan\delta = 0.002$ at 10 GHz).

The measured radiation patterns are shown in Fig. 10. The boresight cross-polarisation levels in E- and H-planes remain below 30 dB in each frequency band. The sidelobe levels in the E-plane are much higher, in the order of 9–10 dB down from the main beam, than that

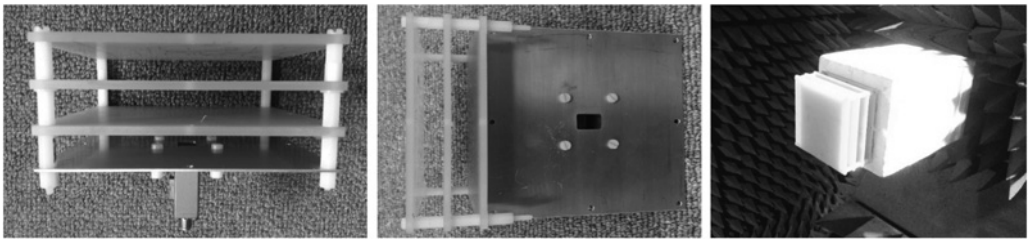

Fig. 8 *Photographs of the prototype ERA. Superstructure is constructed using 3.175 mm-thick FR4 slabs ($\epsilon_r = 4.4$, $\tan\delta = 0.02$ at 10 GHz) and its dimensions are 110×110 mm^2. Commercial waveguide-to-coax adapter feeds the slot aperture behind the aluminium ground plane. Slot dimensions are 14×9.2 mm^2*

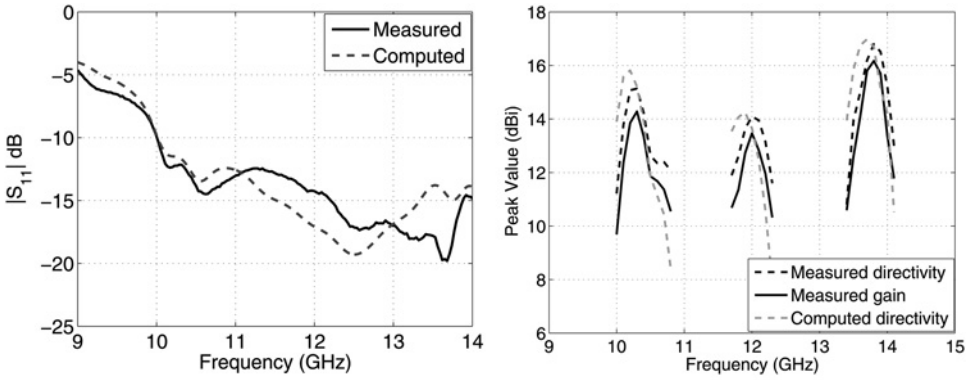

Fig. 9 *Measured input reflection coefficient and gain of the ERA with the slot feed*

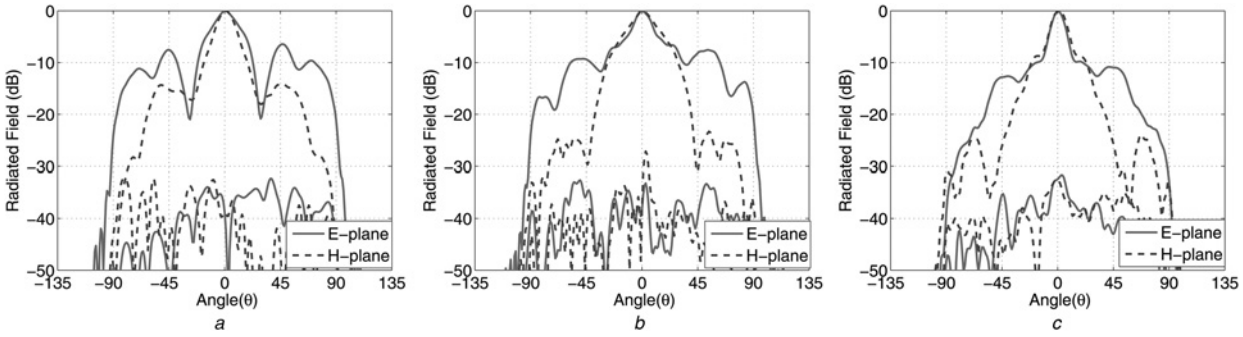

Fig. 10 *Measured radiation patterns of the ERA with the slot feed*

a 10.2 GHz
b 11.9 GHz
c 13.7 GHz

in the *H*-plane. This can be attributed partly to the slot feed and non-uniform aperture phase distribution above the superstructure. Nevertheless, these results confirm the successful design and implementation of a functional tri-band ERA. The total antenna height is 47 mm which is nearly $1.6\lambda_1$, where λ_1 corresponds to free-space wavelength at the first resonance frequency (f_1). When a low antenna profile is important, thin FSS-type superstructures [26] can be used to reduce the antenna height but at the expense of increased design complexity and higher fabrication tolerances.

The proposed ERA can find potential application in 2.5/3.5/5 GHz WiFi/WiMAX extenders and repeaters that provide 14–15 dBi gain. Furthermore, such ERAs based on all-dielectric 1D superstructures are very suitable for dual-linear and circular polarisation applications due to their symmetry [27, 28].

6 Conclusion

We have, by using a 1D superstructure made out of three identical unprinted dielectric slabs, successfully demonstrated a method to design a novel tri-band EBG resonator antenna with simple configuration. We explained how only two resonant defects in a classical superstructure configuration are enough to make the superstructure suitable for tri-band antenna operation given that its reflection phase is engineered correctly at three distinct frequency bands. Simultaneous use of unit-cell SM and DCM provided useful insight into the working principle of the antenna. Full-wave antenna simulations revealed the possibility to tune the frequency ratios (f_2/f_1 and f_3/f_1) in the range of 1.10–1.20 and 1.30–1.38, respectively, given the slabs have identical thickness and permittivity. The design methodology may be modified to achieve independent control of the three frequency bands.

The antenna performance is affected by the type of feed used. Although three individual patch antennas, one for each band to separately feed the cavity, resulted in the best overall directivity/gain values, a slot feed with one input connector is a better option for practical applications. However, higher sidelobe levels can be a limitation. Hence, a more optimal planar feed with improved performance is desirable.

7 References

1 Cheype, C., Serier, C., Thevenot, M., *et al.*: 'An electromagnetic bandgap resonator antenna', *IEEE Trans. Antennas Propag.*, 2002, **50**, (9), pp. 1285–1290
2 Guerin, N., Enoch, S., Tayeb, G., *et al.*: 'A metallic Fabry–Perot directive antenna', *IEEE Trans. Antennas Propag.*, 2006, **54**, (1), pp. 220–224
3 Feresidis, A.P., Vardaxoglou, J.C.: 'High gain planar antenna using optimised partially reflective surfaces', *IEE Proc. Microw. Antennas Propag.*, 2001, **148**, (6), pp. 345–350
4 Weily, A.R., Esselle, K.P., Sanders, B.C., *et al.*: 'High-gain 1D EBG resonator antenna', *Microw. Opt. Technol. Lett.*, 2005, **47**, (2), pp. 107–114
5 Trentini, G.V.: 'Partially reflecting sheet arrays', *IRE Trans. Antennas Propag.*, 1956, **4**, (4), pp. 666–671
6 Pirhadi, A., Keshmiri, F., Hakkak, M., *et al.*: 'Analysis and design of dual band high directive EBG resonator antenna using square loop FSS as superstrate layer', *Prog. Electromagn. Res.*, 2007, **70**, pp. 1–20
7 Lee, Y.J., Yeo, J., Mittra, R., *et al.*: 'Application of electromagnetic bandgap (EBG) superstrates with controllable defects for a class of patch antennas as spatial angular filters', *IEEE Trans. Antennas Propag.*, 2005, **53**, (1), pp. 224–235
8 Al-Tarifi, M.A., Anagnostou, D.E., Amert, A.K., *et al.*: 'Bandwidth enhancement of the resonant cavity antenna by using two dielectric superstrates', *IEEE Trans. Antennas Propag.*, 2013, **61**, (4), pp. 1898–1908
9 Liu, Z., Zhang, W., Fu, D., *et al.*: 'Broadband Fabry–Perot resonator printed antennas using FSS superstrate with dissimilar size', *Microw. Opt. Technol. Lett.*, 2008, **50**, (6), pp. 1623–1627
10 Feresidis, A.P., Vardaxoglou, J.C.: 'A broadband high-gain resonant cavity antenna with single feed'. First European Conf. on Antennas and Propagation (EuCAP), November 2006, pp. 1–5
11 Li, Y., Esselle, K.P.: 'Consideration of bandwidth of the small EBG-resonator antenna using the in-phase highly-reflecting surface'. IEEE Antennas and Propagation Society Int. Symp. (APSURSI), 2009, June 2009, pp. 1–4
12 Weily, A.R., Esselle, K.P., Bird, T.S., *et al.*: 'Dual resonator 1-D EBG antenna with slot array feed for improved radiation bandwidth', *IET Microw. Antennas Propag.*, 2007, **1**, (1), pp. 198–203
13 Rodes, E., Diblanc, M., Arnaud, E., *et al.*: 'Dual-band EBG resonator antenna using a single-layer FSS', *IEEE Antennas Wirel. Propag. Lett.*, 2007, **6**, pp. 368–371
14 Leger, L., Monediere, T., Jecko, B.: 'Enhancement of gain and radiation bandwidth for a planar 1-D EBG antenna', *IEEE Microw. Wirel. Compon. Lett.*, 2005, **15**, (9), pp. 573–575
15 Ge, Y., Esselle, K.P., Bird, T.S.: 'Experimental demonstration of a dual-band electromagnetic band-gap resonator antenna made out of a simple, single-layer frequency selective surface', *Microw. Opt. Technol. Lett.*, 2011, **53**, (8), pp. 1867–1869
16 Leger, L., Granger, R., Thevenot, M., *et al.*: 'Multifrequency dielectric EBG antenna', *Microw. Opt. Technol. Lett.*, 2004, **40**, (5), pp. 420–423
17 Wang, N., Zhang, C., Zeng, Q., *et al.*: 'New dielectric 1-D EBG structure for the design of wideband resonator antennas', *Prog. Electromagn. Res.*, 2013, **141**, pp. 233–248
18 Kelly, J., Passalacqua, G., Feresidis, A.P., *et al.*: 'Simulations and measurements of dual-band 2-D periodic leaky-wave antenna'. Loughboruogh Antennas and Propagation Conf., 2007 (LAPC 2007), April 2007, pp. 293–296
19 Hashmi, R.M., Zeb, B.A., Esselle, K.P.: 'Wideband high-gain EBG resonator antennas with small footprints and all-dielectric superstructures', *IEEE Trans. Antennas Propag.*, 2014, **62**, (6), pp. 2970–2977
20 Weily, A.R., Horvath, L., Esselle, K.P., *et al.*: 'A planar resonator antenna based on a woodpile EBG material', *IEEE Trans. Antennas Propag.*, 2005, **53**, (1), pp. 216–223
21 Zeb, B.A., Ge, Y., Esselle, K.P.: 'A new technique to design 1-D dual-band EBG resonator antennas'. IEEE Antennas and Propagation Society Int. Symp. (APSURSI), July 2011, pp. 1804–1807
22 Zeb, B.A., Ge, Y., Esselle, K.P., *et al.*: 'A simple dual-band electromagnetic band gap resonator antenna based on inverted reflection phase gradient', *IEEE Trans. Antennas Propag.*, 2012, **60**, (10), pp. 4522–4529
23 Zeb, B.A., Ge, Y., Esselle, K.P., *et al.*: 'Reflection phase characteristics of a uniform 1-D EBG superstrate for tri-band directivity enhancement'. Proc. 2011 Microwave and Optical Technology Int. Symp. (ISMOT 2011), June 2011, pp. 187–189
24 Zeb, B.A., Hashmi, R.M., Esselle, K.P., *et al.*: 'The use of reflection and transmission models to design wideband and dual-band Fabry–Perot cavity antennas (invited paper)'. Proc. of 2013 URSI Int. Symp. on Electromagnetic Theory (EMTS), 2013, pp. 1084–1087
25 Weiland, T.: 'RF and microwave simulators – from component to system design'. Proc. of 2003 European Microwave Week (EuMW 2003), pp. 591–596
26 Zeb, B.A., Ge, Y., Eselle, K.P.: 'A single-layer thin partially reflecting surface for tri-band directivity enhancement'. Proc. Asia-Pacific Microwave Conf. (APMC 2012), December 2012, pp. 559–561
27 Zeb, B.A., Eselle, K.P.: 'High-gain dual-band dual-polarised electromagnetic band gap resonator antenna with an all-dielectric superstructure', *IET Microw. Antennas Propag.*, 2015, **9**, (10), pp. 1059–1065
28 Zeb, B.A., Nikolic, N., Esselle, K.P.: 'A high-gain dual-band EBG resonator antenna with circular polarization', *IEEE Antennas Wirel. Propag. Lett.*, 2015, **14**, pp. 108–111